Journal Name

ARTICLE TYPE

Cite this: DOI: 00.0000/xxxxxxxxxx

ELECTRONIC SUPPLEMENTARY INFORMATION
First Hyperpolarizability of Water at the Air-Vapor Interface: A QM/MM Study Questions Standard Experimental Approximations

Guillaume Le Breton*, Oriane Bonhomme*, Pierre-François Brevet*, Emmanuel Benichou* and Claire Loison*‡

Contents

S1 Methodological details **S1**

S2 Interface structure **S4**

S3 Hyperpolarizability **S5**

S4 Susceptibility expressions **S7**

S1 Methodological details

S1.1 QM/MM workflows using the FROG tool.

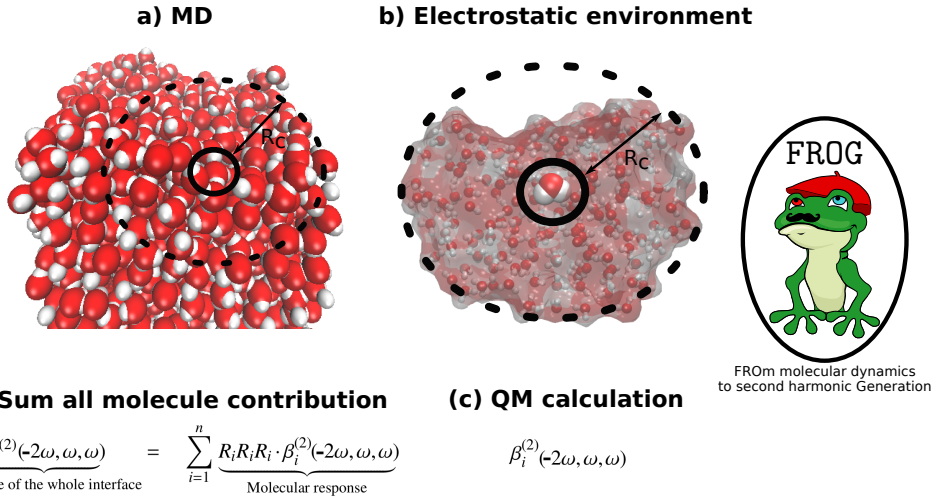

Fig. S1 Scheme of the QM/MM procedure, handled by the FROG script. See the text for more details.

To compute the structural properties of the simulated system, such as the molecular orientations and the hyperpolarizabilities, a home-made software FROG (FROm molecular dynamics to second harmonic Generation) is used. This Python software opens trajectories from MD codes using the module MDAnalysis[1]. First, common structural analyses are performed: molecular orientation (see

* University of Lyon, Université Claude Bernard Lyon 1, CNRS, Institut Lumière Matière, F-69622, Villeurbanne, France
‡ Corresponding author. E-mail : claire.loison@univ-lyon1.fr

Figure 5(b) or S4), or H-bond network (see Figure S3). Then, for each molecule located nearby the interface, the neighborhood at a given time step is built up to a distance R_c, see Figure S1 **(a)**. From the structural environment, an electrostatic one is built: each of the neighbor molecule is described using the same point charges as in the MD (TIP4P/2005), Figure S1 **(b)**. The electrostatic potential generated by these neighbors is taken into account within the Polarizable Embedding scheme[2,3] of the DALTON software[4], release 2018.2. In practice, the Hamiltonians of individual molecules are different since they depend on the neighborhood. For every configuration, FROG writes the QM input. Individual frequency-dependent hyperpolarizabilities are calculated for every molecule, Figure S1 **(c)**. The QM calculations of the Non Linear Opical (NLO) properties are performed on a cluster. They are still more expensive that the MD run, but distributing them over many cores makes this approach numerically affordable. Finally, FROG analyses the individual QM outputs and compute the altitude-dependent distribution of the hyperpolarizability, Figure S1 **(d)**.

FROG code is available on demand to the corresponding author.

S1.2 Quantum Chemistry Calculations

S1.2.1 Basis set and functional for gas-phase calculations

The impact of basis set and DFT functional on the hyperpolarizability components for water molecule in gas phase are summarized in Table S1. We use the quantity $\beta_{\|}$ to compare with the values of literature[5–7]. The definition of $\beta_{\|}$ is :

$$\beta_{\|} = \frac{\sum_i \beta_i \mu_i}{|\mu|}, \quad \text{with} \quad \beta_i = \frac{1}{5}\sum_j \beta_{ijj} + \beta_{jij} + \beta_{jji}, \tag{S1}$$

and μ_i are the dipole moment components (the permament dipole has been calculated at the DFT level in the gas phase).

The Dunning's correlation consistent (cc) basis sets[8–10] studied here (cc-VTZ, cc-VQZ, aug-cc-VDZ, aug-cc-VTZ, aug-cc-PVTZ and d-aug-cc-pVTZ) include polarization functions. The notations VDZ, VTZ, VQZ mean respectively double, triple and quadruple gaussian functions for each valence atoms. The augmented basis set – noted with aug and d-aug – respectively includes one or two diffuse functions of each angular momentum to represent the electron delocalization. We have added our own results for CCSD/d-aug-cc-pVTZ (performed using Dalton and its default settings).

Table S1 Comparison with literature of hyperpolarizability components for water molecule in gas phase (in atomic unit). Each components are computed for a static field and for a wavelength of 694 nm. The $\beta_{\|}$ is defined in the Eq. S1. Reference notations : [a] is Ref. 6. [b] is Ref. 11. [c] is Ref. 5. [d] is the experimental value of Ref. 7 with its uncertainty. Results without references are our calculations. The absolute error (MAE) averaged of all non-zero β components is given for DFT/d-aug-cc-pVTZ relative to CCSD/d-aug-cc-pVTZ.

	β_{caa}		β_{aca}		β_{cbb}		β_{bcb}		β_{ccc}		$\beta_{\|}$		MAE	
Wavelength	∞	694	∞	694	∞	694	∞	694	∞	694	∞	694	∞	694
B3LYP														
aug-cc-pVTZ	-14.9	-17.4	-14.9	-17.4	-5.0	-4.2	-5.0	-10.2	-11.75	-14.5	-19.0	-24.1		
aug-cc-pVTZ[a]	-14.4	-17.7	-14.4	-17.6	-5.0	-4.3	-5.0	-10.0	-11.2	-14.4	-18.3	-24.1		
d-aug-cc-pVTZ	-11.8	-14.2	-11.8	-14.0	-5.3	-6.5	-5.3	-9.5	-14.7	-18.8	19.1	-24.8	1.1	1.7
CAM-B3LYP														
aug-cc-pVTZ	-13.6	-15.7	-13.6	-15.7	-4.2	-3.5	-4.2	-8.4	-10.3	-12.5	-16.1	-21.0		
aug-cc-pVTZ[a]	-13.0	-15.5	-13.0	-15.5	-4.2	-3.5	-4.2	-8.2	-9.6	-12.0	-16.1	-20.5		
d-aug-cc-pVTZ	-10.6	-12.5	-10.6	-12.4	-4.2	-5.0	-4.2	-7.4	-12.1	-15.3	-16.1	-20.6	1.3	1.3
CCSD														
d-aug-cc-pVDZ[b]											-15.0			
d-aug-cc-pVTZ[b]											-17.9			
d-aug-cc-pVQZ[b]											-18.3			
d-aug-cc-pV5Z[b]											-18.2			
d-aug-cc-pVTZ[c]	-9.9		-9.9		-5.7		-5.7		-14.0					
d-aug-cc-pVTZ	-9.9	-11.5	-9.9	-11.4	-5.7	-6.7	-5.7	-8.5	-14.0	-16.9	-17.7	-21.7	0	0
Exp. ESHG[d]											-22.0 ± 0.9			

The impact of basis set and DFT functional on the hyperpolarizability components for a water molecule in **gas phase** are summarized in ESI Table S1, and compared to calculated or experimental values of literature[5–7]. The results obtained with the d-aug-cc-pVTZ basis set are considered as satisfactory.

S1.2.2 Bulk liquid phase calculations

The impact of the basis set on the β components and on $|\beta|$ for water in the bulk phase is depicted in Fig. S2, with

$$|\beta| = \left(\sum_{i,j,k} \beta_{ijk}^2 \right)^{\frac{1}{2}}. \tag{S2}$$

The value of β is calculated using DFT (CAM-B3LYP) and an embedding up to $R_c = 2$ nm for about 55 000 configurations. As for the

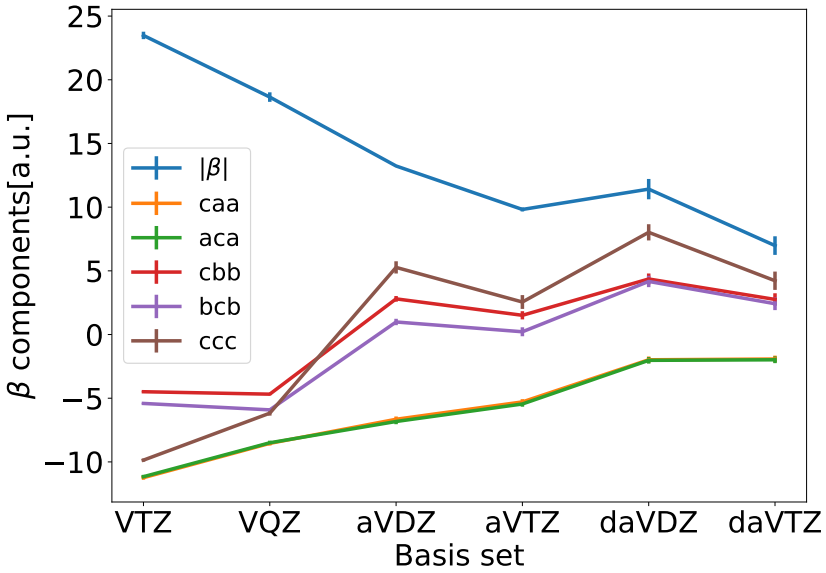

t

Fig. S2 Evolution of β components for several basis set, using DFT with the CAM-B3LYP functional, $R_c = 20$ Å , at 800 nm. $|\beta|$ is defined by Eq. S2.

gas phase, polarization and diffuse function basis set are necessary, and we have chosen to use the d-aug-pVTZ in the our work. The relative smooth convergence of the first hyperpolarizability as a function of the basis set permits to gain confidence in the absence of the "spill-out" effect which can appear using QM/MM approaches with large basis sets[12,13].

The averages and standard deviations of the β components within our response scheme in liquid water phase are compared to literature results in Table S2. Both calculation schemes use the TIP4P/2005 rigid force field, $R_c = 15$ Å and the basis is d-aug-pVTZ. Liang et al. have used Couple-Cluster calculation (CCSD), while we have used DFT.

Table S2 Molecular SHG first hyperpolarizability $\beta(-2\omega, \omega, \omega)$ for $\omega = 0$ of Liang et al.[5] using CCSD(left column), compared to our CAM-B3LYP results CAM-B3LYP (right column), both using the d-aug-pVTZ basis set. Hyperpolarizabilities are in atomic units. Standard deviations are provided in brackets.

	Liquid	
λ	∞[5]	∞
β_{caa}	-2.06 [1.06]	-1.87 [1.01]
β_{cbb}	1.59 [1.83]	2.43 [1.74]
β_{ccc}	3.00 [3.04]	3.80 [2.82]
β_{bbb}	0.00 [5.74]	0.00 [5.21]
β_{bcc}	0.00 [1.64]	0.01 [1.2]
β_{baa}	0.00 [1.38]	-0.01 [1.31]
β_{aaa}	0.00 [1.56]	0.01 [1.47]
β_{abb}	0.00 [1.64]	0.00 [1.56]
β_{acc}	0.00 [1.13]	0.01 [1.11]
β_{abc}	0.00 [0.78]	0.00 [0.85]

S1.3 Error Bars

Error bars Δ for any quantity X were computed as follow:

$$V[X] = \frac{1}{N}\sum_{n=1}^{N}(X_n)^2 - \left(\frac{1}{N}\sum_{n=1}^{N}X_n\right)^2 , \text{ and} \qquad \Delta[X] = \sqrt{\frac{V[X]}{N_f \times S}} , \tag{S3}$$

where X can be the orientation of a water molecule or components of β tensor. N stands for the total number of configurations (individual calculations) considered for the average value, i.e. for all molecules of all the frames treated – typically several tens of thousands. For the altitude profiles, the N configurations describe molecules within XY-slices of thickness of a few angstrom. N_f stands for the number of different time steps treated (typically 32 and 80 for bulk and interface respectively). These are considered as independent with respect to the SHG response (see main text Section 2.3). S stands for a geometrical factor taking into account possible spatial correlations between water molecules which are close to each other.

We have considered that molecules distant from more than 0.8 nm are independent with respect to their NLO properties. Therefore, the system can be divided into small sub-box of 1.6 nm per side. For the bulk phase, these sub-boxes are $1.6\times1.6\times1.6$ nm^3 cubes. At the interface they are $1.6\times1.6\times0.1$ nm^3 parallelepipeds (X, Y, Z directions) since the response is discretized along the Z direction. Thus, for the bulk phase, using box size in nm, $S = (\text{size of the MD box}/1.6)^3$ and for the interface $S = (\text{size of the MD box along } xy/1.6)^2$. For the bulk phase $\sqrt{S} = 6$ and at the interface $\sqrt{S} = 3$.

S2 Interface structure

Figure S3 reports the number of given and accepted H-bonds per water molecule, as a function of the altitude, i.e. the position relative to the liquid-vapor interface along the Z-direction.

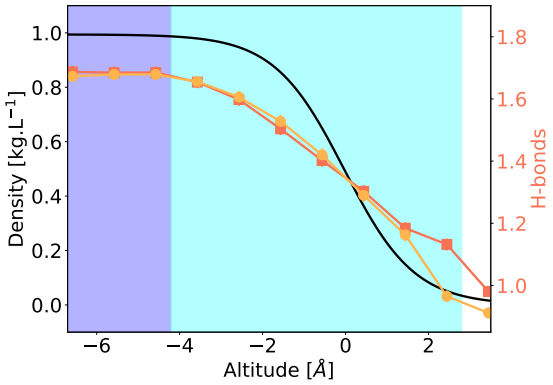

Fig. S3 Number of given and accepted H-bonds per water molecule, as a function of the altitude $\Delta Z = Z - Z_0$, where Z_0 is the average position of the interface. Squares and circles are used for the average accepted and given H-bonds, respectively. The errors bars are calculated using Eq S3. Hyperbolic tangent water density fit in dark solid line.

Figure S4 reports the orientational order parameter P_2 of the water dipole moment relative to the normal of the liquid-vapor interface: $P_2 = \langle \frac{1}{2}(3\cos^2\theta - 1)\rangle$, where $\theta = (c, Z)$. $P_2 \simeq 0$ in the bulk indicates an isotropic distribution. $P_2 \simeq 1$ indicates a propensity to align along the surface normal ($\pm Z$). $P_2 \simeq -1/2$ indicates a propensity to align parallel to the surface. We measure negative values and conclude that the dipole moment of the water molecule show a propensity to align parallel to the surface.

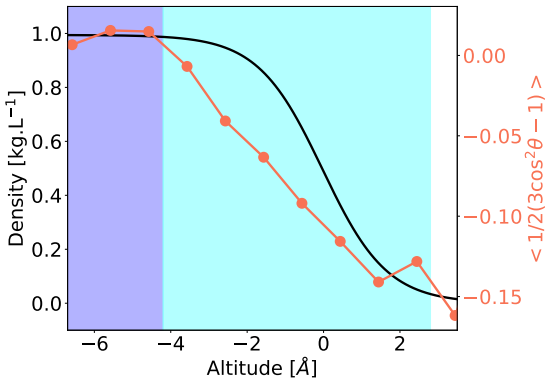

Fig. S4 Orientational order parameter of the water dipole moment as a function of the altitude $\Delta Z = Z - Z_0$, where Z_0 is the average position of the interface. Hyperbolic tangent water density fit in dark solid line.

S3 Hyperpolarizability

In this section, we complete the methodological tests presented in the main text on the number of configurations needed form averaging N_f, and the radius of the electrostatic environment R_c.

S3.1 Convergence relative to the number of configurations

This section provide supplementary information concerning the convergence of the β components relative to the value obtained with largest frame number (80 frames, 4294 water molecules in total) for a chosen altitude ($Z - Z_0 = -0.6 \pm 0.5$ Å) for which the density is about half the bulk density.

The Figure S5 depicts the C_{2v} forbidden components, which converges within ± 0.05 atomic unit after 2000 configurations.

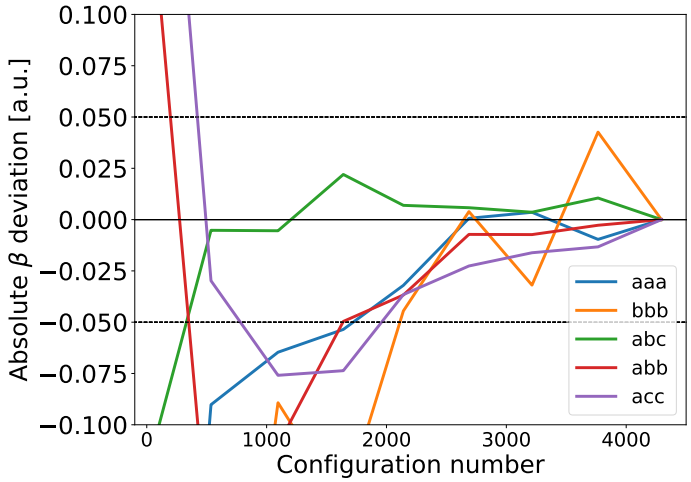

Fig. S5 Evolution of the β C_{2v} forbidden components mean value in atomic unit with respect to the reference value obtained using 4294 molecular configurations. The dashed line represent 0.05 a.u. deviation.

Using 4000 configurations (80 frames for our systems size) lead to converged results. Overall, the statistical error made by this configuration number should be smaller than the one made by our choice of QM method – DFT instead of CCSD for instance. Note that because of the density evolution with the altitude, the number of molecular configurations available decreases for increasing altitudes. At altitudes higher than ($Z - Z_0 = -0.6$ Å), *i.e.* closer to the vapor phase, our hyperpolarizability values are less precise.

In total, 48 650 hyperpolarizability calculations were necessary for the Main-Text-Figure 7. They have cost approximately 11 k-hours for a single 2.6 Ghz CPU.

S3.2 Electrostatic embedding : R_c convergence

This section provides supplementary information concerning the convergence of the β components relative to the size of the embedding environment R_c. Beyond a given distance, the electrostatic field generated by the surrounding no longer affects the mean β value.

S3.2.1 Bulk phase

Figure S6 depicts the deviation of the β component mean values for several R_c, with respect to the results obtain with $R_c = 2$ nm. 48 000 configurations have been used per R_c. The C_{2v} forbidden components are not shown since their mean value are zero for all R_c. From 1.0 to 1.5 nm, an important evolution is observed for all the non-zero components while between 1.5 and 2.0 nm, there is almost no evolution. Therefore, an R_c of 2.0 nm seems sufficient to converge the hyperpolarizability components in the water bulk phase for our PE0-TIP4P/2005 scheme.

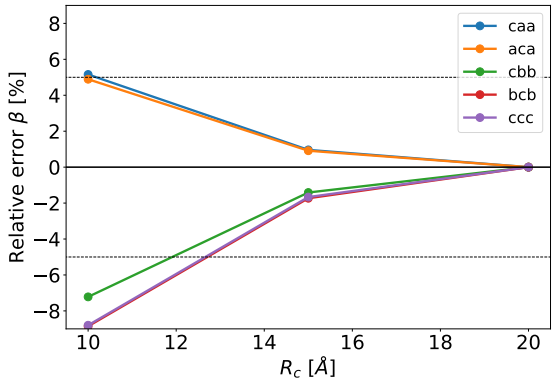

Fig. S6 Relative evolution of the β components in the bulk phase for several R_c with respect to the results obtain with $R_c = 2.0$ nm.

S3.2.2 At the interface:

As for the time-convergence, the evolution of the mean β as a function of the R_c has not been computed for all the altitudes but only at one: $Z - Z_0 = -0.6 \pm 0.5$ Å. 80 frames have been used for each R_c to ensure time-convergence. The Figure S7 shows the evolution of the relative mean β with respect to R_c for the non-zero components. The components forbidden by the C_{2v} water symmetry remains null in averaged for all R_c (data not shown). As for the bulk phase, an R_c about 2.0 nmm is sufficient to converge the averaged β. We have studied the convergences of β for slices at other altitudes, and the results are similar – data not shown.

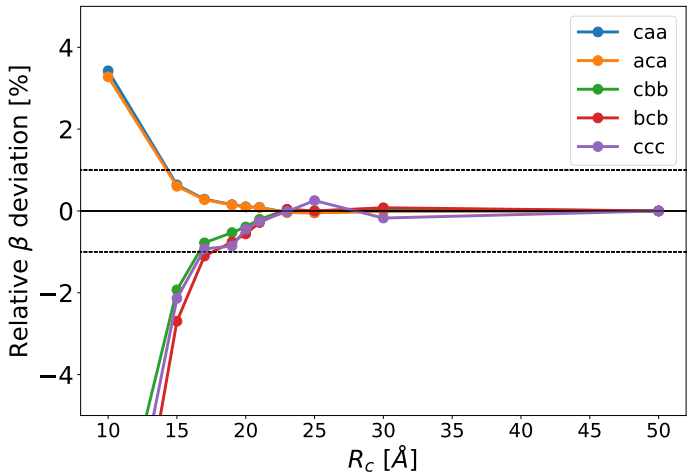

Fig. S7 Evolution of the non-zero $\beta(-2\omega,\omega,\omega)$ components with respect to the R_c using the relative deviation compared to the results obtained for $R_c = 5.0$ nm at the altitude $\Delta Z = -0.06$ nm. The exciting wavelength is 800 nm. The dashed black lines represent a deviation of ± 1 %. The norms of the C_{2v} forbidden components are all bellow 0.3 atomic units for all R_c.

S4 Susceptibility expressions

To discuss relevant orientation/hyperpolarizability correlations, we recall here common expressions of the surface susceptibility components for the S-SHG from neat air/water interface considering only the dipolar contribution, as can be found in Refs. 6,14–16.

The molecular frame has the c-axis along the C_{2v} axis of the water molecule, $\{a,c\}$ contains the three atoms. The water molecule belongs to C_{2v} symmetry, with seven non-zero polarizability tensor elements in SHG : β_{ccc}, β_{caa}, β_{cbb}, $\beta_{aac}=\beta_{aca}$, $\beta_{bbc}=\beta_{bcb}$. For the C_∞ neat air/water interface, there are seven non-zero elements, for the surface susceptibility tensor $\chi^{(2)}$: χ_{ZZZ}, $\chi_{ZXX}=\chi_{ZYY}$, $\chi_{XZX}=\chi_{YZY}=\chi_{XXZ}=\chi_{YYZ}$.

Considering the twisted angle ψ and the azimuthal angle ϕ as isotropic and uncorrelated with the β tensor elements yields expressions found in Ref. 6 :

$$\begin{aligned}
\chi^{(2)}_{ZXX} &= \frac{N}{4}\left\{2\left\langle(\beta_{caa}+\beta_{cbb})\cos\theta\right\rangle+\left\langle(2\beta_{ccc}-\beta_{caa}-\beta_{cbb}-2\beta_{aca}-2\beta_{bcb})\cos\theta\sin^2\theta\right\rangle\right\},\\
\chi^{(2)}_{XZX} &= \frac{N}{4}\left\{2\left\langle(\beta_{aca}+\beta_{bcb})\cos\theta\right\rangle+\left\langle(2\beta_{ccc}-\beta_{caa}-\beta_{cbb}-2\beta_{aca}-2\beta_{bcb})\cos\theta\sin^2\theta)\right\rangle\right\},\\
\chi^{(2)}_{ZZZ} &= \frac{N}{4}\left\{2\left\langle\beta_{ccc}\cos^3\theta\right\rangle+\left\langle(\beta_{caa}+\beta_{cbb}+2\beta_{aca}+2\beta_{bcb})\cos\theta\sin^2\theta\right\rangle\right\}.
\end{aligned}\tag{S4}$$

where N is the number of molecules. If one defines intermediate values

$$\beta'_\perp = \beta_{caa}+\beta_{cbb},\tag{S5}$$

$$\beta''_\perp = \beta_{aca}+\beta_{bcb},\tag{S6}$$

$$\beta_\perp = \frac{1}{2}\left(\beta'_\perp+2\beta''_\perp\right).\tag{S7}$$

It simplifies to :

$$\begin{aligned}
\chi^{(2)}_{ZXX} &= \frac{N}{2}\left\{\left\langle\beta'_\perp\cos\theta\right\rangle+\left\langle(\beta_{ccc}-\beta_\perp)\cos\theta\sin^2\theta\right\rangle\right\},\\
\chi^{(2)}_{XZX} &= \frac{N}{2}\left\{\left\langle\beta''_\perp\cos\theta\right\rangle+\left\langle(\beta_{ccc}-\beta_\perp)\cos\theta\sin^2\theta)\right\rangle\right\},\\
\chi^{(2)}_{ZZZ} &= \frac{N}{2}\left\{\left\langle\beta_{ccc}\cos^3\theta\right\rangle+\left\langle\beta_\perp\cos\theta\sin^2\theta\right\rangle\right\}.
\end{aligned}\tag{S8}$$

Noticeably, these expressions neglect C_{2v}-forbidden elements. In our calculations, the averages of these elements are null at all altitudes (see Main Text Figure 6).

S4.1 Neglecting orientation/hyperpolarizability correlations

Now, the common assumption $\langle\beta_{ijk}\cos^l\theta\rangle=\langle\beta_{ijk}\rangle\langle\cos^l\theta\rangle$ is considered. This assumption allows to extract the molecule's orientation from the S-SHG signal in many studies. Equation S8 simplifies to:

$$\begin{aligned}
\chi^{(2)}_{ZXX} &= \frac{N}{2}\left\{\left\langle\beta'_\perp\right\rangle\left\langle\cos\theta\right\rangle+\left\langle(\beta_{ccc}-\beta_\perp)\right\rangle\left\langle\cos\theta\sin^2\theta\right\rangle\right\},\\
\chi^{(2)}_{XZX} &= \frac{N}{2}\left\{\left\langle\beta''_\perp\right\rangle\left\langle\cos\theta\right\rangle+\left\langle(\beta_{ccc}-\beta_\perp)\right\rangle\left\langle\cos\theta\sin^2\theta)\right\rangle\right\},\\
\chi^{(2)}_{ZZZ} &= \frac{N}{2}\left\{\left\langle\beta_{ccc}\right\rangle\left\langle\cos^3\theta\right\rangle+\left\langle\beta_\perp\right\rangle\left\langle\cos\theta\sin^2\theta\right\rangle\right\}.
\end{aligned}\tag{S9}$$

S4.2 Taking into account altitude variations

Equations S8 can be rewritten to take into account variations of $\langle\beta_{ijk}\cos^l\theta\rangle$ or density ρ as a function of the altitude $Z-Z_0$ (see Figure 5). The susceptibility is the sum over the whole system, which can be decomposed into slices of different positions Z[6]. Equations S8

become:

$$\begin{aligned}
\chi^{(2)}_{ZXX} &= \frac{A}{2}\int_Z \left\{ \langle \beta'_\perp \cos\theta \rangle_Z + \left\langle (\beta_{ccc}-\beta_\perp)\cos\theta\sin^2\theta \right\rangle_Z \right\} \rho(Z) dZ, \\
\chi^{(2)}_{XZX} &= \frac{A}{2}\int_Z \left\{ \langle \beta''_\perp \cos\theta \rangle_Z + \left\langle (\beta_{ccc}-\beta_\perp)\cos\theta\sin^2\theta) \right\rangle_Z \right\} \rho(Z) dZ, \\
\chi^{(2)}_{ZZZ} &= \frac{A}{2}\int_Z \left\{ \left\langle \beta_{ccc}\cos^3\theta \right\rangle_Z + \left\langle \beta_\perp \cos\theta\sin^2\theta \right\rangle_Z \right\} \rho(Z) dZ.
\end{aligned} \tag{S10}$$

Where the notation $\langle\cdot\rangle_Z$ corresponds to the averaging over molecules situated in a slab parallel to the interface, characterized by its position Z and its thickness dZ. In our work, dZ is 1 Å. The part between curly brackets of Equation S10, $\{\langle\beta_{ccc}\cos^3\theta\rangle_Z + \langle\beta_\perp\cos\theta\sin^2\theta\rangle_Z\}$, is plotted in Main-Text-Figure 9 (blue squares).

Similarly, Equations S9 neglecting orientation/hyperpolarizability correlations become:

$$\begin{aligned}
\chi^{(2)}_{ZXX} &= \frac{A}{2}\int_Z \left\{ \langle \beta'_\perp \rangle_Z \langle \cos\theta \rangle_Z + \langle \beta_{ccc}-\beta_\perp \rangle_Z \left\langle \cos\theta\sin^2\theta \right\rangle_Z \right\} \rho(Z) dZ, \\
\chi^{(2)}_{XZX} &= \frac{A}{2}\int_Z \left\{ \langle \beta''_\perp \rangle_Z \langle \cos\theta \rangle_Z + \langle \beta_{ccc}-\beta_\perp \rangle_Z \left\langle \cos\theta\sin^2\theta) \right\rangle_Z \right\} \rho(Z) dZ, \\
\chi^{(2)}_{ZZZ} &= \frac{A}{2}\int_Z \left\{ \langle \beta_{ccc} \rangle_Z \left\langle \cos^3\theta \right\rangle_Z + \langle \beta_\perp \rangle_Z \left\langle \cos\theta\sin^2\theta \right\rangle_Z \right\} \rho(Z) dZ.
\end{aligned} \tag{S11}$$

The part between curly brackets of Equation S11 has been plotted in Main-Text-Figure 9 (red circles).

The experimental S-SHG signal is proportional to the integral. Whereas the Z-dependency of the density can be guessed, the evolution of the NLO-part is not known. To extract molecular information from experimental data, it is often assumed that the S-SHG signals emerge from an 'one-layer' system, i.e. the integrand is independent of Z.

S4.3 Molecular Kleinman symmetry

In the numerical calculations, we observe that the average hyperpolarizability tensor almost respects the Kleinman symmetry throughout the interface, see Figure 7. Therefore, we shall suppose in the following that for all altitudes,

$$\langle \beta''_\perp \rangle_Z \simeq \langle \beta'_\perp \rangle_Z, \tag{S12}$$

$$\langle \beta'_\perp \rangle_Z \simeq \frac{2}{3}\langle \beta_\perp \rangle_Z. \tag{S13}$$

Which remains true if one neglects the Z dependence.

For our system, using (Eq. S12), neglecting both Z-dependance and orientation/hyperpolarizability correlations, Equations S11 become

$$\chi^{(2)}_{XZX} \simeq \chi^{(2)}_{ZXX}, \tag{S14}$$

$$\begin{aligned}
\chi^{(2)}_{ZXX} &= \frac{N}{2}\left\{ \beta'_\perp \langle\cos\theta\rangle + (\beta_{ccc}-\beta_\perp)\left\langle \cos\theta\sin^2\theta \right\rangle \right\}, \\
\chi^{(2)}_{ZZZ} &= \frac{N}{2}\left\{ \beta_{ccc}\left\langle \cos^3\theta \right\rangle + \beta_\perp \left\langle \cos\theta\sin^2\theta \right\rangle \right\}.
\end{aligned} \tag{S15}$$

Where $\langle\beta_{ijk}\rangle$ is noted β_{ijk} for simplicity. The difference between $\chi^{(2)}_{XZX}$ and $\chi^{(2)}_{ZXX}$ observed experimentally is not explained using this formalism.

S4.4 Link with the molecular orientation parameter

Equations S15 are straightforwardly equivalent to :

$$\begin{aligned}
\chi^{(2)}_{ZXX} &\simeq \frac{N}{2}\left\{ \left(\beta_{ccc}-\frac{1}{3}\beta_\perp\right)\langle\cos\theta\rangle + (\beta_\perp-\beta_{ccc})\left\langle\cos^3\theta\right\rangle \right\}, \\
\chi^{(2)}_{ZZZ} &= \frac{N}{2}\left\{ \beta_\perp\langle\cos\theta\rangle + (\beta_{ccc}-\beta_\perp)\left\langle\cos^3\theta\right\rangle \right\}.
\end{aligned} \tag{S16}$$

Noting α the ratio between β_{ccc} and $\beta_\perp$ with $\beta_\perp = \alpha\beta_{ccc}$, then

$$\begin{aligned}
\chi^{(2)}_{ZXX} &= \frac{N}{2}\beta_{ccc}\left\{\frac{3-\alpha}{3}\langle\cos\theta\rangle + (\alpha-1)\left\langle\cos^3\theta\right\rangle\right\},\\
\chi^{(2)}_{ZZZ} &= \frac{N}{2}\beta_{ccc}\left\{\alpha\langle\cos\theta\rangle + (1-\alpha)\left\langle\cos^3\theta\right\rangle\right\}.
\end{aligned} \tag{S17}$$

Within this framework, neglecting the altitude dependence, knowing the ratio α, and measuring the experimental observable χ, one typically studies the molecular orientation parameter D (e.g. Refs. 14,17):

$$D = \frac{\left\langle\cos^3\theta\right\rangle}{\langle\cos\theta\rangle}.$$

Note that some authors use the inverse as a definition of molecular orientation parameter[15]. If one supposes here α different from 1, then :

$$D = \frac{\alpha\,\chi_{ZXX} - (1-\alpha/3)\,\chi_{ZZZ}}{(\alpha-1)(\chi_{ZXX}+\chi_{ZZZ})}. \tag{S18}$$

Results of our calculations question such a framework:

- $\alpha = \beta_\perp/\beta_{ccc}$ varies through the interface, see Figure 7.
- At several altitudes, the common approximation $\langle\beta_{ijk}\,\cos^l\theta\rangle = \langle\beta_{ijk}\rangle\langle\cos^l\theta\rangle$ does not hold. Figure 9 shows the difference for the NLO part of the integrand in $\chi^{(2)}_{ZZZ}$, with and without this assumption.

Notes and references

1 N. Michaud-Agrawal, E. J. Denning, T. B. Woolf and O. Beckstein, *J. Comput. Chem.*, 2011, **32**, 2319–2327.
2 J. M. Olsen, K. Aidas and J. Kongsted, *J. Chem. Theory Comput.*, 2010, **6**, 3721–3734.
3 C. Steinmann, P. Reinholdt, M. S. Nørby, J. Kongsted and J. M. H. Olsen, *Int. J. Quantum Chem.*, 2019, **119**, e25717.
4 K. Aidas, C. Angeli, K. L. Bak, V. Bakken, R. Bast, L. Boman, O. Christiansen, R. Cimiraglia, S. Coriani, P. Dahle *et al.*, *Wiley Interdisciplinary Reviews: Computational Molecular Science*, 2014, **4**, 269–284.
5 C. Liang, G. Tocci, D. M. Wilkins, A. Grisafi, S. Roke and M. Ceriotti, *Phys. Rev. B*, 2017, **96**, 1–6.
6 T. T. Pham, A. Jonchère, J. F. Dufrêche, P. F. Brevet and O. Diat, *J. Chem. Phys.*, 2017, **146**, 144701.
7 D. P. Shelton and J. E. Rice, *Chemical Reviews*, 1994, **94**, 3–29.
8 R. A. Kendall, T. H. Dunning and R. J. Harrison, *J. Chem. Phys.*, 1992, **96**, 6796–6806.
9 D. E. Woon and T. H. Dunning, *J. Chem. Phys.*, 1993, **98**, 1358–1371.
10 D. E. Woon and T. H. Dunning, *J. Chem. Phys.*, 1994, **100**, 2975–2988.
11 P. Beaujean and B. Champagne, *The Journal of Chemical Physics*, 2016, **145**, 044311.
12 P. Reinholdt, J. Kongsted and J. M. H. Olsen, *J. Phys. Chem. Lett.*, 2017, **8**, 5949–5958.
13 C. Steinmann, P. Reinholdt, M. S. Nørby, J. Kongsted and J. M. H. Olsen, *Int. J. Quantum Chem.*, 2019, **119**, e25717.
14 P.-F. Brevet, *Surface Second Harmonic Generation*, PPUR presses polytechniques, 1997.
15 W.-k. Zhang, D.-s. Zheng, Y.-y. Xu, H.-t. Bian, Y. Guo and H.-f. Wang, *J. Chem. Phys.*, 2005, **123**, 224713.
16 M. N. Nasir, E. Benichou, C. Loison, I. Russier-Antoine, F. Besson and P.-F. Brevet, *Phys. Chem. Chem. Phys.*, 2013, **15**, 19919–19924.
17 A. G. F. de Beer and S. Roke, *J. Chem. Phys.*, 2010, **132**, 234702.